Catal Lett (2012) 142:213–217
DOI 10.1007/s10562-011-0741-9

Characterization of Nanostructured Silica*Cat* Pd^0

Valerica Pandarus · Rosaria Ciriminna · Francois Béland · Piera Demma Carà · Mario Pagliaro

Received: 29 August 2011 / Accepted: 10 November 2011 / Published online: 24 November 2011

Abstract Structural investigation on nanostructured Silia*Cat* Pd^0 palladium catalyst sheds light into the origins of the remarkable activity of these new catalytic materials.

Keywords Palladium · ORMOSIL · Silia*Cat* · Cross-coupling · Nanoparticle

1 Introduction

Sol–gel silica-based catalysts doped with catalytic species have lately emerged as a powerful chemical technology [1, 2]. In this field, the new catalyst series Silia*Cat* Pd^0 (Silia*Cat* is a trademark of SiliCycle, Inc.) made of nanostructured Pd^0 organosilica xerogels was recently reported for application to truly heterogeneous carbon–carbon coupling [3], debenzylation [4] and hydrogenation [5] of functionalized nitroarenes reactions.

Palladium-catalyzed carbon–carbon bond formation (cross-coupling) reactions such as those named after Suzuki–Miyaura, Mizoroki–Heck, Negishi and Sonogashira developed over the last 30 years have changed the practice of synthetic organic chemistry from a linear pattern of slow, consecutive reaction steps with protected substrates into the parallel synthesis of key precursors that are eventually then linked together at a late stage in the process [6]. This is possible because these reactions generally tolerate the presence of functional groups in the coupling partners, and thus do not require tedious protection and deprotection steps of functional groups in the reagents.

Homogeneous cross-coupling reactions, however, have several shortcomings such as limited reusability of the expensive catalyst, which impacts cost, and palladium contamination in the product [7]. Removing residual palladium—for instance with silica-based scavengers [8]—provides a challenging task for chemists in the pharmaceutical and fine chemicals industry to reduce its content to the demanding maximum acceptable concentration limit requirements of drugs regulators.

Before Silia*Cat* Pd^0 no efficient sol–gel entrapped ligand-free Pd^0 catalyst for synthetic organic chemistry was commercially available. Classical sol–gel encapsulation based on hydrolytic polycondensation of silicon alkoxides, indeed, releases large amounts of alcohols that rapidly reduce the Pd(II) precursor to catalytically inactive bulk Pd^0 (palladium black), whereas only nanostructured Pd is able to mediate C–C coupling reactions [9]. This is not the case of Silia*Cat* Pd^0 and here we describe the results of a structural investigation aimed to elucidate the origin of the remarkable activity of these new catalytic materials.

2 Results and Discussion

A whole series of different 75%-methyl modified ORMOSIL (organically modified silicate) catalysts doped with Pd^0 nanocrystals were prepared according to the alcohol-free sol–gel synthetic methodology described elsewhere [3], involving polycondensation of $MeSi(OEt)_3$ and $Si(OEt)_4$ precursors (Eq. 1):

V. Pandarus · F. Béland (✉)
SiliCycle Inc., 2500, Parc-Technologique Blvd, Quebec, QC G1P 4S6, Canada
e-mail: FrancoisBeland@silicycle.com

R. Ciriminna · P. D. Carà · M. Pagliaro (✉)
Istituto per lo Studio dei Materiali Nanostrutturati, CNR, via U. La Malfa 153, Palermo 90146, Italy
e-mail: mario.pagliaro@cnr.it

$$\mathrm{Si(OEt)} + \mathrm{MeSi(OEt)_3} + \mathrm{Pd^2} + \mathrm{H_2O} \xrightarrow{-\mathrm{EtOH,reduction}} \mathrm{Pd@[Me\text{-}SiOnHm(OEt)q]p} \quad (1, \text{unbalanced})$$

An alcohol-free sol undergoes further basic catalyzed polycondensation to yield a mesoporous hydrogel that is dried to afford a xerogel doped with Pd^{2+}. The latter material is eventually treated with a mild reductant to yield nanostructured encaspulated catalyst Silia*Cat* Pd^0. The metal load in each catalyst in Table 1 was measured using a CAMECA SX100 instrument equipped with EPMA analyzer suitable for non-destructive elemental analysis of micron-sized volumes at the surface of materials, with ppm sensitivity. The SEM pictures of the Silia*Cat* Pd^0 catalysts reveal the typical matrix structure of organosilica particles made of homogeneous particles with diameter sizes in the range from 60 to 125 μm.

The amorphous nature of the $MeSiO_{1/2}$ undoped material (prepared in our laboratory) [10] acting as entrapping catalyst matrix was confirmed by the characteristic wide XRD diffractogram (Fig. 1a). The dopant palladium crystallites, however, are made of crystalline Pd^0 nanoparticles. This is clearly shown by the XRD pattern of the powder in which the crystalline nature of the active nano-phase is evident from the succession of peaks (Table 2; Fig. 1b) characteristic of the face centered cubic structure of metallic Pd, for which a typical 5.7 nm (for Silia*Cat* Pd^0**-4**) metallite particle size was calculated using the Scherrer equation [11] from the line broadening of the (111) reflection.

The Pd particle sizes of all the other catalysts studied were <6 nm, with increasingly smaller particles with decreasing palladium load. The smallest Pd crystallite size (3.2 nm) is observed for Silia*Cat* Pd^0**-1** catalyst that, remarkably, showed the highest catalytic activity in all cross-coupling, debenzylation and hydrogenation reactions in which it was employed.

2.1 FTIR

Figure 2 shows that no significant changes in absorption IR spectra of Silia*Cat* Pd^0**-1** are observed before and after two consecutive catalytic runs in Suzuki cross-coupling of 4-iodo-nitrobenzene and phenylboronic acid carried out in methanol under reflux, which is in agreement with the fact that these catalysts exhibit unprecedented stability among Pd heterogeneous catalysts and can be reused several times to achieve high coupling conversions [3] without any additional activation treatment.

Table 1 Textural properties and load of Silia*Cat* Pd^0 catalysts (adapted from Ref. [2], with permission)

Sample	Pd loading (mmol g^{-1})	Surface (m^2 g^{-1})	Pore size range (Å)
Silia*Cat* Pd^0**-1**	0.03	754	40.00
Silia*Cat* Pd^0**-2**	0.112	774	45.00
Silia*Cat* Pd^0**-3**	0.148	724	48.75
Silia*Cat* Pd^0**-4**	0.163	721	52.50

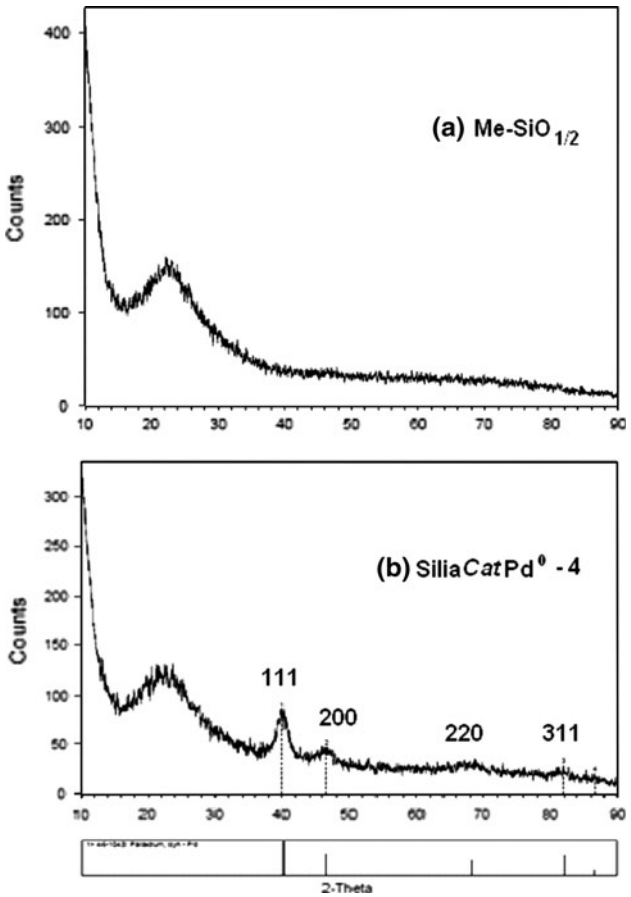

Fig. 1 Powder X-ray diffraction (XRD) pattern of Silia*Cat* Pd^0**-4** catalyst

The dominant peaks characteristic of the Si–O bond oscillations [12, 13] are the main higher frequency band at about 1,020 cm^{-1} ascribed to the symmetric stretching, accompanied by the bands at 1,117 cm^{-1} and 771 cm^{-1} due, respectively, to the asymmetric and symmetric stretching of the O atoms. The signals of the $–CH_3$ groups attached to Si atoms are evident by the characteristic sharp band at 1,270 cm^{-1} due to the symmetric deformation vibration of the CH_3 group, and at 2,976 cm^{-1} due to stretching vibration of C–H bonds [14].

2.2 Textural Properties

Nitrogen adsorption and desorption isotherms at 77 K were measured using a Micrometrics TriStar™ 3000 system, analyzing the resulting data with the Tristar™ 3000 4,01

Table 2 X-ray powder diffraction (XRD) of Silia*Cat* Pd^0**-4**

Catalyst	Diffraction angle 2θ				Mean crystallite size[b] (nm)
	111	200	220	311	
[a]Pd^0	40.12	46.66	68.12	82.10	N.A.
Silia*Cat* Pd^0**-4**	39.96	46.66	68.11	81.90	5.7

[a] The Powder Diffraction File of The International Centre for Diffraction Data is used to identified the diffractions peaks characteristic of crystalline Pd^0 with a face centered cubic (fcc) lattice identified Pd^0

[b] Calculated from XRD using Debye–Scherrer equation: $d = K\lambda/\beta \cos\theta$

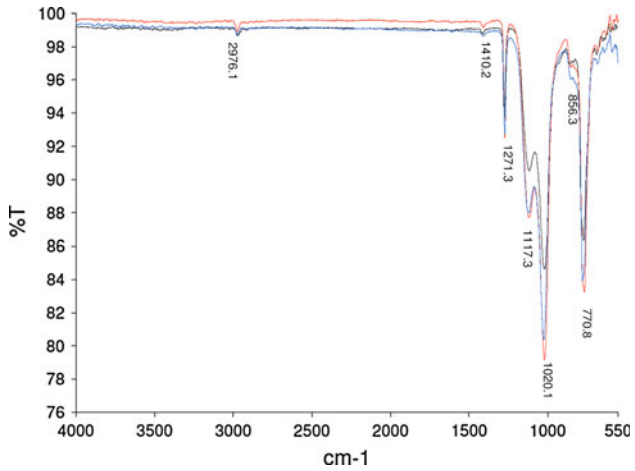

Fig. 2 IR spectra of Silia*Cat* Pd^0**-1** heterogeneous catalyst before (*red*) and after one (*blue*) and two (*black*) catalytic runs in Suzuki cross-coupling of 4-iodo-nitrobenzene and phenylboronic acid carried out in methanol under reflux. The spectra were obtained at room temperature using an ABB Bomem MB series FTIR spectrometer at a resolution of 4 cm^{-1} and taking 30 scans per spectrum in the range of 4,000–550 cm^{-1}

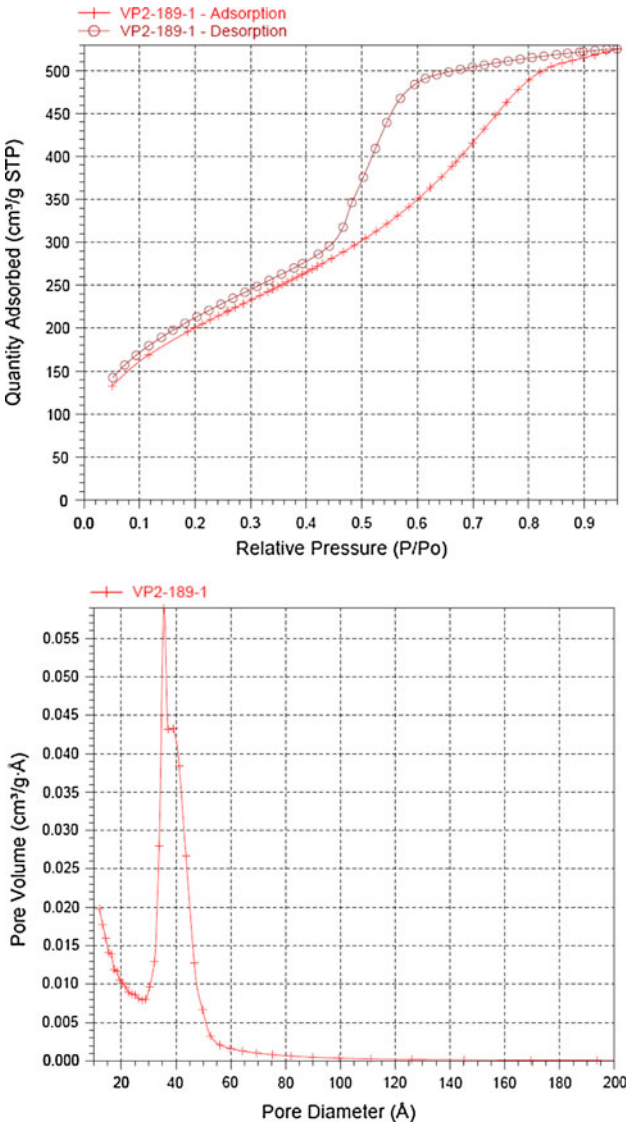

Fig. 3 N_2-adsorption and desorption isotherms and pore volume distribution of Silia*Cat* Pd^0**-1**

software (both adsorption and desorption branches were used to calculate the pore size distribution). The type IV N_2-adsorption isotherms of all Silia*Cat* Pd^0 catalysts (showing only Silia*Cat* Pd^0**-1** in Fig. 3) are typical of mesoporous materials [15] with large BET surface area (>720 m^2 g^{-1}) and a narrow pore size distribution of mesopores capable to adsorb a considerable volume of cryogenic nitrogen (>0.84 cm^3 g^{-1}).

The H1 type hystereses observed for all catalysts, furthermore, are characteristic of solids consisting of particles made by consolidated aggregates of spheroidal particles with pores of uniform size and shape from which evaporation takes place at a pressure lower than that of capillary condensation, due to different size of pore mouth and pore body [15].

Results in Table 3 indicate that the textural properties of the catalysts are only slightly changing (with modest increase in the surface area and pore volume) going from Silia*Cat* Pd^0**-1** through Silia*Cat* Pd^0**-4**, namely increasing the amount of water and NaOH condensation catalyst in the sol–gel process of Eq. 1.

This is due to the elimination of ethanol from the alcogel mixture resulting in a hydrogel in which the capillary tension at the cage solid–liquid interface is greatly reduced preventing collapse of the gel during drying [16]. Furthermore, elimination of EtOH favours alkoxide monomers

Table 3 Textural properties of the Silia*Cat* Pd^0 catalysts

Catalyst	SSA ($m^2\ g^{-1}$)	SPV ($cm^3\ g^{-1}$)	Pore size (Å)
Silia*Cat* Pd^0-**1**	753	0.844	30.83
Silia*Cat* Pd^0-**2**	773	0.926	32.96
Silia*Cat* Pd^0-**3**	723	0.891	34.70
Silia*Cat* Pd^0-**4**	720	0.939	36.65

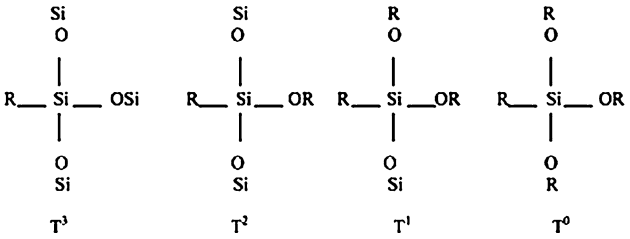

Fig. 4 ^{29}Si Solid state NMR analysis. Species in the T^n representation system

hydrolysis and slows down condensation so that rapid aggregation of the early sol particles is prevented and $CH_3Si(OEt)_3$ can fully hydrolyse to CH_3–$Si(OH)_3$ and this copolymerize with the $Si(OH)_4$ monomers derived by the faster TEOS hydrolysis. The outcome is an organosilica amorphous matrix with covalently bounded methyl groups homogeneously distributed in an open the silica-based network in which most of the added Pd nanophases are encapsulated at the surface of the hydrophobic silica mesopores, and thus accessible for catalysis.

2.3 Solid State NMR

For all catalysts the ^{29}Si NMR spectra were collected and analyzed according to the chemical shifts known as the T^n Si sites, where T designates the presence of 3 oxygen first neighbors and the exponent n (0–4) designates the number of Si second neighbors (Fig. 4) [17].

The spectra of Silia*Cat* Pd^0-**1** and Silia*Cat* Pd^0-**4** are shown in Fig. 5. The degree of cross-linking of different catalysts displayed in Table 4 takes into account the contribution of various silicon species present in the matrix, according to Eq. 2: [18]

$$\text{Degree of cross-linking} = \left[\left(\text{area } T^1 + 2\times \text{ area } T^2 + 3\times \text{ area } T^3\right)/3\right] \times 100\% \quad (2)$$

The degree of cross-linking apparently does not correlate with catalytic activity, such as in the case of lipase-containing ORMOSILs [19]. Likewise, the specific surface area and the pore size do not seem to be the decisive factor in determining the relative Pd nanophase activities of the Pd^0 containing hybrid gels.

We ascribe the highest catalytic activity of Silia*Cat* Pd^0-**1** catalyst with the smallest Pd crystallite size (3.2 nm) to the fact that smaller nanoparticles possess a higher degree of curvature, weakening the bonding of their surface atoms, and higher surface energies due to metal–metal bond deficiency of the surface atoms which results in instability and enhanced chemical activity of the surface atoms [20]. A similar increase in selective activity with decreasing crystallite size has been observed, for example, for Heck coupling reactions mediated by Pd^0 on carbon [21].

However, other factors beyond metal dispersion influence the overall reactivity of these materials. The sol–gel entrapment of Pd isolated metallic nanophase within the ORMOSIL matrix sol–gel cages ensures three concomitant advantages. First, it allows entrapment and stabilization of ultra-small crystalline Pd nanoparticles protecting them also from Ostwald ripening (growth in the size of the nanoparticles, highly detrimental for catalysis) [21]. Second, the strongly lipophilic nature of the ORMOSIL matrix ensures preferential adsorption of the less-reactive (lipophilic) moiety of the substrate dictating preferential access of the reactive -I groups of 4-iodobenzene to the phenyl boronic acid molecules adsorbed on the Pd nanoparticles (Fig. 6).

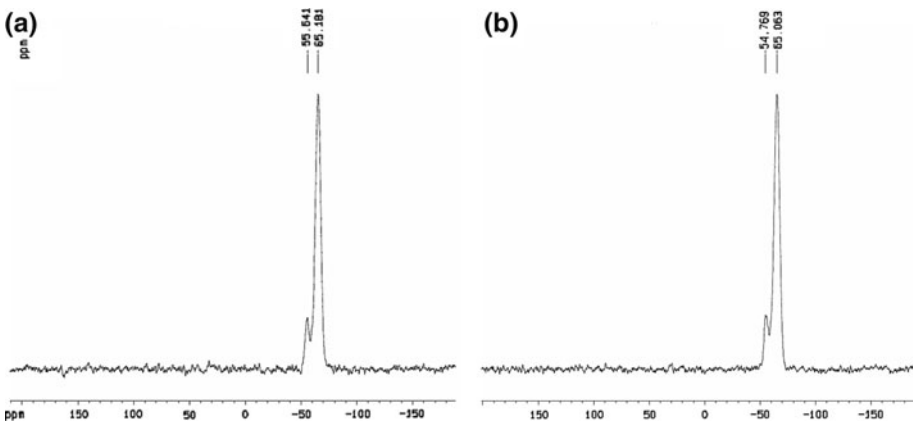

Fig. 5 NMR ^{29}Si spectra of Silia*Cat* Pd^0-**1** (**a**) and of Silia*Cat* Pd^0-**4** (**b**) heterogeneous catalysts

Table 4 ^{29}Si NMR parameters of the Silia*Cat* Pd^0 catalysts

Catalyst	T_1 ppm	T_2 ppm	T_3 ppm	Degree of cross-linking (%)
Literature[Ref] [17]	−46 to −49	−55 to −58	−62 to −70	–
$MeSiO_{1/2}$[a]	0	−55.58	−66.38	11.7
Silia*Cat* Pd^0-**1**	0	−55.64	−65.18	11.6
Silia*Cat* Pd^0-**2**	0	−55.78	−65.32	11.2 (a value)
Silia*Cat* Pd^0-**3**	0	−55.58	−65.27	14.1
Silia*Cat* Pd^0-**4**	0	−54.76	−65.06	11.9

Silica spectra were recorded on a Bruker Avance spectrometer (Milton, ON) at a silicon frequency of 79.5 MHz. Samples are spun at 8 kHz at magic angle at room temperature in a 4 mm ZrO rotor. A Hahn echo sequence synchronized with the spinning speed is used while applying a TPPM15 composite pulse decoupling during acquisition. 2,400 acquisitions are recorded with a recycling delay of 30 s

[a] Silica gel support without palladium

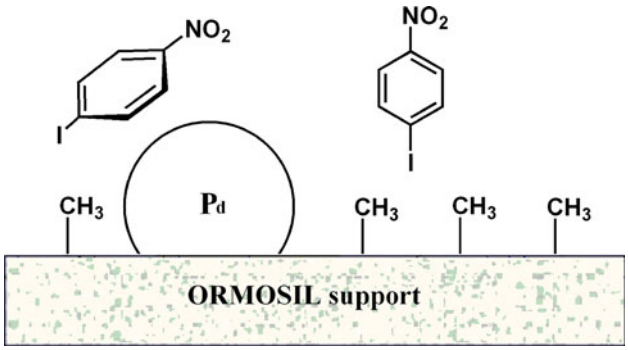

Fig. 6 Schematic representation of adsorbed 4-iodobenzene on a hydrogen saturated Silia*Cat* Pd^0—hydrogel catalyst

Third, the well known hydrophobic nature of fully alkyl-modified silica xerogels ensures continuous lack of adsorbed water at the material's cage surface [22], that usually leads to secondary by-products formation as observed with most common commercial supported Pd catalysts. Accordingly, organosilica Silia*Cat* Pd^0 can be safely applied for mediating the Sonogashira and Suzuki coupling reactions to give coupled products in high yield and selectivity without the need to exclude air or moisture [3].

Again, this is in agreement with knowledge about nanostructured catalytic xerogels produced from ORMOSILS [23]. Pd nanoparticles sol–gel entrapped in unmodified hydrophilic SiO_2, for example, showed only poor activity in most cross-coupling reactions (data not shown).

Finally, Silia*Cat* Pd^0 differs from previously developed palladium heterogeneous technologies because nanostructured Pd^0 is the only active species (no ligand is employed) whereas the chemically and physically stable organosilica matrix ensures unprecedented stability and ease of use. A number of new applications of this multipotent catalyst technology are emerging that, in light of the numerous practical advantages, are likely to find soon industrial application.

Acknowledgments This article is dedicated to Dr Antonio Tombolini for all he has done for a wise and positive use of the Internet in Italy in all these years. We thank Mr. Pierre Audet for ^{29}Si NMR spectra, Mr. Marc Choquette for microsonde analysis and Mr. Jean Frenette for XRD analysis, all from Laval University (Québec); and Mr. Pierre-Gilles Vaillancourt and Mr. Stéphane Houle from QC Department of SiliCycle Inc. for their valuable contribution.

References

1. Ciriminna R, Carà PD, Sciortino M, Pagliaro M (2011) Adv Synth Catal 353:677
2. Marr AC, Marr PC (2011) Dalton Trans 40:20
3. Pagliaro M, Pandarus V, Béland F, Ciriminna R, Palmisano G, Carà PD (2011) Catal Sci Technol. doi:10.1039/C1CY00119A
4. Pandarus V, Béland F, Ciriminna R, Pagliaro M (2011) Chem Cat Chem 3:xx
5. Pandarus V, Ciriminna R, Béland F, Pagliaro M (2011) Catal Sci Technol 1:xx
6. Barnard C (2008) Platinum Metals Rev 52:38
7. Rouhi AM (2004) Chem Eng News 82(36):49
8. Garrett CE, Prasad K (2004) Adv Synth Catal 346:889
9. Reetz MT, de Vries JG (2004) Chem Commun 35:1559
10. Ciriminna R, Pagliaro M, Palmisano G et al. (2010) Patent WO/2010/015081. 11 February 2010
11. Sangeetha P, Seetharamulu P, Shanthi K, Narayanan S, Rao KSR (2007) J Mol Catal A Chem 273:244
12. Galeener EG (1979) Phys Rev B 19:4292
13. Park ES, Ro HW, Nguyen CV, Jaffe RL, Yoon DY (2008) Chem Mater 20:1548
14. Brown JF, Vogt LH, Prescott PI (1964) J Am Chem Soc 86:1120
15. Leonfanti G, Padovan M, Tozzola G, Venturelli B (1998) Catal Today 41:207
16. De Witte BM, Commers D, Uytterhoeven JB (1996) J Non Cryst Solids 202:35
17. Glaser RH, Wilkes GL, Bronnimann CE (1989) J Non Cryst Solids 113:73
18. Sugahara Y, Okada S, Sato S, Kuroda K, Kato C (1994) J Non Cryst Solids 167:21
19. Noureddini H, Gao X (2007) J Sol Gel Sci Technol 41:31
20. Narayanan R, Tabor C, El-Sayed MA (2008) Top Catal 48:60–74
21. Köhler K, Heidenreich RG, Krauter JGE, Pietsch J (2002) Chem Eur J 8:622
22. Fidalgo A, Ciriminna R, Ilharco LM, Pagliaro M (2005) Chem Mater 17:6686
23. Ciriminna R, Ilharco LM, Fidalgo A, Campestrini S, Pagliaro M (2005) Soft Matter 1:231